Atmos. Chem. Phys. Discuss., 8, 10227–10255, 2008
www.atmos-chem-phys-discuss.net/8/10227/2008/

Atmospheric Chemistry and Physics Discussions

Influence of modelled soil biogenic NO emissions on related trace gases and the atmospheric oxidizing efficiency

J. Steinkamp[1], **L. N. Ganzeveld**[2], **W. Wilcke**[3], **and M. G. Lawrence**[1]

[1]Department of Atmospheric Chemistry, Max-Planck-Institute for Chemistry, Mainz, Germany
[2]Department of Environmental Sciences, Chairgroup Earth System Sciences, Wageningen University and Research Centre, Wageningen, Netherlands
[3]Geographic Institute, Johannes Gutenberg University, Mainz, Germany

Received: 22 April 2008 – Accepted: 2 May 2008 – Published: 30 May 2008

Correspondence to: J. Steinkamp (steinkam@mpch-mainz.mpg.de)

Published by Copernicus Publications on behalf of the European Geosciences Union.

Abstract

The emission of nitric oxide (NO) by soils (SNOx) is an important source of oxides of nitrogen (NO_x=NO+NO_2) in the troposphere, with estimates ranging from 4 to 21 Tg of nitrogen per year. Previous studies have examined the influence of SNOx on ozone (O_3) chemistry. We employ the ECHAM5/MESSy earth system model to go further in the reaction chain and investigate the influence of SNOx on lower tropospheric NO_x, O_3, peroxyaceltyl nitrate (PAN), nitric acid (HNO_3), the hydroxyl radical (OH) and the lifetime of methane (τ_{CH_4}). We show that SNOx is responsible for a significant contribution to the NO_x mixing ratio in many regions, especially in the tropics. On the other hand in some regions SNOx has a negative feedback on the lifetime of NO_x through O_3 and OH, which results in regional increases in the mixing ratio of NO_x despite lower total emissions in a simulation without SNOx. Furthermore, the concentration of OH is substantially increased due to SNOx, resulting in an enhanced oxidizing efficiency of the global troposphere, reflected in a ~10% decrease in τ_{CH_4} due to soil NO emissions.

1 Introduction

Nitric oxide (NO) in the soil is produced by the microbial processes of nitrification and denitrification (Firestone and Davidson, 1989). The NO emission originates from a natural pool of nitrogen and a fraction from fertilizer application (Yienger and Levy II, 1995; Stehfest and Bouwman, 2006). The estimates of NO emitted yearly by soils (hereafter called SNOx) ranges from 4 to 21 Tg(N) (Yienger and Levy II, 1995; Davidson and Kingerlee, 1997, and references therein). NO reacts rapidly with other atmospheric compounds, establishing an equilibrium between NO and nitric dioxide (NO_2). These two species are frequently refered to the oxides of nitrogen (NO_x). SNOx is topped by the anthropogenic combustion of fossil fuels (20–24 $\frac{\text{Tg(N)}}{\text{yr}}$) (Holland et al., 1999) and is comparable to the production of NO_x from lightning and biomass burning, but especially in remote continental regions of the mid- and low-latitudes SNOx is the dom-

ACPD

8, 10227–10255, 2008

inant source of NO_x. Through reactions, deposition and stomatal uptake directly within the vegetation layer not all NO emitted by the soil escapes the canopy layer as NO_x (Yienger and Levy II, 1995; Ganzeveld et al., 2002b). In this work SNOx refers to the flux from the vegetation to the atmosphere. The fraction of NO_x that reaches the atmosphere reacts as a catalyst for production of ozone (O_3), one of the greenhouse gases. This O_3 production is driven by the oxidation of carbon monoxide (CO) and volatile organic compounds (VOC), if the concentration of NO is higher than about 5–30 $\frac{\text{pmol}}{\text{mol}}$ (Brasseur et al., 1999). Atmospheric NO_x is also involved in the production of the hydroxyl radical (OH), which is responsible for the oxidation and depletion of methane (CH_4), another greenhouse gas. Beyond these climate related issues, high NO_x mixing ratios also have a direct impact on human health. NO_x is removed from the atmosphere by reaction with hydroxyl radicals (OH) or oxidation to dinitrogen pentaoxide (N_2O_5) and subsequent deposition as nitric acid (HNO_3). It can also react with organic tracers to form peroxyl nitrates, mainly peroxyacetyl nitrate (PAN), which, once it is lifted to higher altitudes, can be transported over large distances releasing NO_x when it is transported back downward again.

Previous model studies of the influence of SNOx on atmospheric chemistry mainly focused either on the NO_x source itself, or on O_3, mostly on a regional scale. Jaeglé et al. (2005) examined the global partitioning of NO_x sources using inverse modelling and the space-based NO_2 column derived by GOME (Global Ozone Monitoring Experiment). Their a posteriori SNOx ($8.9\frac{\text{Tg(N)}}{\text{yr}}$) is 68% greater than their a priori SNOx ($5.3\frac{\text{Tg(N)}}{\text{yr}}$). Based on this, Jaeglé et al. (2005) suggest that the influence of SNOx on background O_3 could be underestimated in current chemistry transport models (CTMs). Bertram et al. (2005) come to a similar conclusion by inverse modelling using another satellite sensor (SCIAMACHY) above the western United States, computing an underestimation of 60%. Delon et al. (2007) modelled higher O_3 concentrations with higher SNOx above Western Africa. For Europe, Simpson (1995) found that SNOx hardly has any influence on controling the O_3 mixing ratio. Isaksen and Hov (1987) already investigated the influence of changes in the emission intensity of different relevant trace gases

on the oxidizing efficiency through an increase in OH concentration with increased NO_x emissions, but they neglected SNOx.

In this study, we take these analyses a step further and follow the reaction chain from SNOx through O_3 and OH to its global influence on the oxidizing efficiency of the atmosphere. To do so, we compare two model runs with a state-of-the-art global 3-D global chemistry climate model. One is a simulation with all relevant emissions and reactions (BASE), and the second simulation is without SNOx (NOBIONO = "No biogenic NO"). We expect a considerable influence of SNOx on the mixing ratios and distribution of related global tropospheric trace gases (NO_x, PAN, HNO_3, O_3 and OH). Furthermore the global oxidizing efficiency, indicated by the lifetime of CH_4 (τ_{CH_4}), is expected to decrease (τ_{CH_4} increases) if we exclude NO_x emission from soils.

In the following section we briefly describe the model setup. We then compare the relevant tracer mixing ratios from the BASE simulation versus the NOBIONO simulation. In the final section we present our conclusions and outlook.

2 Model description and setup

For this study the Modular Earth Submodel System version 1.2 (MESSy) coupled to the general circulation model ECHAM5 is employed. MESSy connects, through a standardized interface, submodels for different processes with bidirectional feedbacks (Jöckel et al., 2005, 2006). The meteorology for these simulations is driven by sea surface temperature (SST) from the AMIPIIb dataset (Taylor et al., 2000). The calculation of SNOx in the BASE simulation is based on the algorithm of Yienger and Levy II (1995), which is the most widely used SNOx algorithm in CTMs (Ganzeveld et al., 2002a; Jaeglé et al., 2005; Delon et al., 2007). This calculation is performed in the submodel EMDEP (Ganzeveld et al., 2006). NO_x produced by lightning is calculated in the submodel LNOX (2.2 $\frac{Tg(N)}{yr}$). The remaining sources of NO_x (49 $\frac{Tg(N)}{yr}$) are read in from the offline EDGAR database (Olivier et al., 1994) by the submodel OFFLEM (Kerkweg et al., 2006). Other relevant emissions are calculated either by the EMDEP

ACPD
8, 10227–10255, 2008

or OFFLEM submodel.

A model spinup time of eleven months (Janurary–November 1994) was chosen and the data of the period December 1994–December 1995 is analysed here. To achieve an identical meteorology of both simulations feedback through trace gases and water vapor is switched off. Table 1 recapitulates the setup of the two simulations.

3 Results and discussion

The emission of NO from soils in the BASE simulation accounts for 15% of the total annual global NO emissions (Table 2). The interannual variability of SNOx is low in the model (Steinkamp, 2007). The largest emissions are calculated for tropical regions. During JJA there are some exceptions further north in northern America, Europe and north-eastern China. These are fertilizer induced emissions in agricultural regions (Fig. 1 and Table 2).

The data is analysed by season with a focus on the winter and summer season. There is a notable seasonal variation with larger SNOx in the summer period of each hemisphere and with a larger contribution of SNOx to the total NO emissions during the northern hemispheric spring and summer (Table 2). The first point can be explained by the temperature dependence and the second one by the greater landmasses in the Northern Hemisphere. In the northern mid-latitudes SNOx plays a less important role relative to other NO_x emissions, except during the JJA period.

3.1 Influence of SNOx on related trace gases

The column mean mixing ratios of NO_x, PAN, HNO_3 and O_3 and the column mean concentration of OH in the gridcells (weighted by the air mass in the gridcells) in the lower troposphere (below 500 hPa; hereafter "LT") from the BASE simulation are compared with the values from the NOBIONO simulation.

As expected, in the LT the difference between the NO_x column mean mixing ratio in the NOBIONO simulation versus the BASE simulation is well-correlated with SNOx in

ACPD
8, 10227–10255, 2008

all regions (Table 3). A low correlation is computed for the Northern Hemisphere during DJF, as could be expected due to the small SNOx compared to the anthropogenic emissions.

In the low-latitudes and in the northern mid-latitudes the correlation between SNOx and the difference in the PAN column mean mixing ratio of the two simulations is low (Table 3). This is likely due to the stronger dependence of PAN formation on VOC mixing ratios than on NO_x mixing ratios (Singh et al., 1986). In contrast, there is a much better correlation in the southern mid-latitudes between the difference in the LT PAN column mixing ratio and SNOx. This suggests a dominating role of NO_x in the formation of PAN in the mid-latitudes of the Southern Hemisphere. This hypothesis is partially confirmed by the calculation of the correlation coefficient of the difference in the PAN column mixing ratio with SNOx up to a lower altitude (750 hPa). R^2 increases slightly for the northern mid- and low-latitudes and stays nearly the same for the southern mid-latitudes (Table 3). In the low-latitudes, convective downdrafts and subsiding airmasses, combined with the strong temperature dependence of the decomposition of PAN decreases the correlation.

The correlation between SNOx and the difference in the LT O_3 column mean mixing ratio is lower than for NO_x. This is partly due to the longer lifetime of O_3, which is better mixed in the LT. Furthermore the production of O_3 is not only determined by the NO_x mixing ratio, but also by the concentration of VOC. The correlation of the OH column mean concentration difference in the LT with SNOx is similar to O_3. OH is a very short lived tracer, whose production depends on the one hand on the photolysis of O_3 and the water vapor concentration and on the other hand on the reaction of NO with HO_2 in the troposphere. This results, depending on the dominating reaction, in a higher or lower correlation of the OH column concentration difference versus SNOx than the O_3 column mixing ratio difference versus SNOx.

3.1.1 NO_x

The global mean mixing ratio of NO_x in the LT during DJF decreases by 6% in the NOBIONO simulation compared to the BASE simulation. During JJA it decreases by 12%. In both cases the decrease in the mixing ratio is less than the contribution of SNOx (12% and 17% respectively). The maximum decrease is 78% in DJF and 68% in JJA, while the maximum absolute decreases in the DJF and JJA periods are 139 and 209 $\frac{\text{pmol}}{\text{mol}}$, respectively (figures with absolute differences can be found in the supplement: http://www.atmos-chem-phys-discuss.net/8/10227/2008/acpd-8-10227-2008-supplement.pdf).

Interestingly, during DJF the mixing ratio above large parts of the Northern Hemisphere even increases by up to 3.5% (Fig. 2a), with the largest absolute increase of 15.2 $\frac{\text{pmol}}{\text{mol}}$ above Europe. In the JJA period the maximum relative increase of 4.8% is larger than in the DJF period, but the maximum absolute difference is only 3.0 $\frac{\text{pmol}}{\text{mol}}$ (Fig. 2b).

A similar result has been noted for model sensitivity simulations with and without NO_x from lightning (Stockwell et al., 1999; Labrador et al., 2005), in which a decrease in near surface NO_x mixing ratios was computed for similar regions with increasing production of NO_x by lightning. Although NO_x produced by lightning is formed in the free troposphere and SNOx originates from the surface, we achieve comparable results with SNOx. To explain why the NO_x mixing ratio decreases less than the relative decrease in the emission of the NOBIONO simulation compared to the BASE simulation, and why it increases during the DJF period in large areas in the Northern Hemisphere, the feedback through O_3 and OH has to be taken into account. Stockwell et al. (1999) assumed that the general increase in O_3 with lightning NO_x causes an increase in OH. This OH reduces the lifetime of NO_x (τ_{NO_x}) through Eq. (1) above regions with high non-lightning NO_x sources. Labrador et al. (2005) showed that the conversion to HNO_3 via N_2O_5 also contributes to the shorter τ_{NO_x} (Eq. 2) with higher NO_x emissions.

$$NO_2 + OH \rightarrow HNO_3 \quad (1)$$

$$NO_2 + O_3 \rightarrow NO_3 + O_2 \quad (2a)$$
$$NO_3 + NO_2 \rightarrow N_2O_5 \quad (2b)$$
$$N_2O_5 + H_2O \rightarrow 2\,HNO_3 \quad (2c)$$

$$2\,NO_2 + O_3 + H_2O \rightarrow 2\,HNO_3 + O_2 \quad (2)$$

Similarly we find that without SNOx, O_3 and OH levels decrease, resulting in enhanced τ_{NO_x}, and due to Eqs. (1) and (2) the NO_x mixing ratio increases in regions with low SNOx. The changes in HNO_3, O_3 and OH related to this are discussed in the following sections.

In the vertical direction the strongest effects of SNOx are simulated near the surface (DJF: 53%, JJA: 42%), and a decrease of up to 10 to 25% for higher altitudes in the zonal mean is calculated if SNOx was switched off (Fig. 3). The effect of convective transport to higher altitudes has a stronger influence on the difference in the total burden between 500 and 250 hPa during DJF (relative: 11.3%, absolute: 1.85 Gg) than during JJA (relative: 6.5%, absolute: 1.22 Gg). This is because the main regions, where the convective transport is most effective, are in the Southern Hemisphere especially the Amazon Basin and the southern tropics of Africa (not shown).

3.1.2 PAN

The LT PAN mixing ratio decreases globally by 4% during DJF and 8% during JJA without SNOx. In both periods the PAN mixing ratio decreases nearly everywhere above the continents (Fig. 4). Above the tropical oceans, especially during JJA, there is a high relative but a negligible absolute increase in the PAN mixing ratio associated with a decrease in SNOx. As mentioned above, the formation of PAN in the northern mid- and low latitudes relies more on VOC than on NO_x, but more on NO_x in the southern mid-latitudes. This explains the larger decrease during DJF than during JJA. There is

also no increase of PAN in the Northern Hemisphere during DJF despite higher NO_x mixing ratios, which confirms a dominating role of VOC in PAN formation.

Interestingly, in the upper troposphere between 500 hPa and 250 hPa the largest decrease in the PAN mixing ratio is during DJF (7%), whereas it is 5% during JJA. In the zonal mean of the relative difference in PAN mixing ratio with and without SNOx (Fig. 5), the effect of convective transport in the lower latitudes is more effective during DJF than during JJA. At the higher altitudes PAN does not increase anymore, due to its longer lifetime resulting in better mixing.

The differences in the PAN mixing ratio should be interpreted with caution, because the model generally overestimates its levels compared to observations (Jöckel et al., 2006), though this may improve with a new isoprene oxidation scheme (Butler, personal communication).

3.1.3 HNO_3

The global LT mixing ratio of HNO_3 decreases by 16% (DJF) and 15% (JJA) without SNOx. The greatest decrease occurs above continental regions of the low-latitudes and in the summer months in the Northern Hemisphere (Fig. 6). The larger decrease in the mixing ratio of HNO_3 compared to the decrease of NO_x mixing ratio is because the formation of HNO_3 is not only determined by the NO_x mixing ratio, but also relies on the mixing ratios of O_3 and OH, which also decrease, as discussed in the following sections.

Nitric acid is mainly deposited on aerosol particles, taken up by cloud water or directly deposited on the earth's surface. The deposition of HNO_3 is decreased by 14% throughout the year without SNOx. During DJF the decrease is 12% and during JJA it is 15%.

3.1.4 O_3

The mixing ratio of O_3 in the NOBIONO simulation compared to the BASE simulation in the LT decreases by 6% in both seasons, with the greatest decline above the conti-

ACPD
8, 10227–10255, 2008

nents (Fig. 7). The maximum relative decrease during DJF is 37% and during JJA it is 28%. The maximum absolute decrease (17.6 $\frac{\text{nmol}}{\text{mol}}$) occurs during DJF above Australia (Fig. 7a). In contrast to what was found for NO_x, there is no region with increasing O_3 mixing ratios. The decrease of the NO_x mixing ratio in the LT during JJA (12%) is less effective in reducing the O_3 mixing ratio than the decrease in the NO_x mixing ratio during DJF (6%). This is because the formation of O_3 through SNOx competes with other strong sources of NO_x during JJA in the Northern Hemisphere, whereas SNOx is relatively much more important for the formation of O_3 during DJF in the Southern Hemisphere. Furthermore, as was noted above for the PAN formation in the Northern Hemisphere the simulated O_3 production may be more dependent on VOC than NO_x.

In the zonal mean distribution (not shown) a similar pattern of the influence of convection can be seen as already discussed for NO_x and PAN. But due to the longer lifetime of O_3 the relative change has only a maximum of 17% in DJF and 14% in JJA. These changes are smaller than for NO_x and are more evenly distributed above all latitudes and also in the vertical direction. In the vertical direction there is, as with the horizontal, no increase in the O_3 mixing ratio throughout the troposphere.

3.1.5 OH

Excluding the contribution of SNOx, the mean OH concentration declines by 10% during DJF and 8% during JJA in the LT. The largest relative decrease is 58% during DJF and 42% during JJA above the tropical land regions. During DJF the decrease is shifted to the southern tropics and to the northern tropics during JJA (Fig. 8). Note that during JJA an absolute increase above the Antarctic region is calculated, but the OH concentration here is less than $1 \times 10^4 \frac{\text{molec}}{\text{cm}^3}$.

The decrease is on the one hand induced directly by NO_x through Eq. (3), and on the other hand indirectly by the lower O_3 mixing ratio, leading to less primary OH production, and therefore in a decrease of the OH concentration in the LT.

$$NO + HO_2 \rightarrow HO + NO_2 \quad (3)$$

The largest relative decrease in the zonal mean concentration of OH is 18% during DJF and 14% during JJA. This maximum of the relative decrease in the OH concentration without SNOx is nearly detached from the surface, despite the surface source of SNOx (Fig. 9). At the surface OH production is mainly related to the reaction of $O(^1D)$ with water, while at higher altitudes it depends more on the reaction of NO with HO_2 (Eq. 3). In the zonal mean the shift to the Southern Hemisphere during DJF is stronger than the shift during JJA to the Northern Hemisphere.

3.2 Influence of SNOx on the oxidizing efficiency

The oxidation of CO and VOC in the atmosphere is mainly driven by OH. As a measure for the oxidizing efficiency of the atmosphere, τ_{CH_4} is calculated for both simulations according to Lawrence et al. (2001). The trend of monthly mean values is depicted in Fig. 10. The mean τ_{CH_4} averaged for one year (December 1994 to November 1995) for the BASE simulation is 7.26 years and 7.93 years for the NOBIONO simulation, a 9.2% increase without SNOx. The maximum prolongation of 0.89 years occurs in December 1994 (10.3%) and January 1995 (10.4%).

The changes in τ_{CH_4} are not equally distributed over the globe. In the southern and low-latitudes the relative influence is noticeably greater than in the northern latitudes (Fig. 11). This agrees with the smaller relative change in the OH concentration in the northern latitudes (Fig. 8). In the vertical direction, the relative changes are slightly larger above 500 hPa, even though the origin of SNOx is at the surface. Beginning from the surface source of SNOx and following the reaction chain from NO_x over O_3 and OH in each step, the relative difference of our two simulations becomes smaller near the surface and larger at higher altitudes. This trend corroborates the larger relative change of the oxidizing efficiency at higher altitudes. However, only ~15% of the absolute amount of CH_4 in the troposphere is oxidized above 500 hPa (Lawrence et al., 2001).

Labrador et al. (2004) modelled a decrease of 15% in τ_{CH_4} in a simulation with 5 Tg(N) NO_x produced by lightning relative to one with no lightning NO_x. Compared to this, SNOx is somewhat less effective in altering the oxidizing efficiency of the atmo-

ACPD
8, 10227–10255, 2008

sphere, which is interesting, given that CH_4 oxidation is more effective near the surface where SNOx is emitted, due to the strong temperature dependence of the reaction of OH with CH_4. The change in the oxidizing efficiency due to lightning NO_x is larger than due to SNOx, even though the total emission rate is lower. This is because at higher altitudes the NO:NO_2 ratio is greater, so that with more NO the NO_x lifetime is not diminished as strongly as near the surface. Furthermore at higher altitudes more NO results in higher OH yields by reaction with HO_2.

4 Conclusions and outlook

The emission of NO from soils plays an important role for chemical reactions in the atmosphere. Lower global mean NO_x mixing ratios without SNOx lead to lower global O_3 mixing ratios in the LT. The lower O_3 mixing ratios result in lower OH concentrations. This results in an enhanced lifetime of NO_x in regions with other dominating sources of NO_x. Hence the NO_x mixing ratios increases in some regions, despite lower emissions when SNOx is neglected in our NOBIONO simulation. From this it follows, that although NO_x is a short-lived tracer it indirectly influences chemical processes in regions with low SNOx through feedback with O_3 and OH. By following the reaction chain up to PAN and HNO_3, we detected a dominating role of SNOx compared to VOC in the mid-latitudes of the Southern Hemisphere. Also by following the reaction chain (SNOx→NO_x→O_3→OH), the magnitude of relative effects are shifted step by step to higher altitudes in the troposphere.

Through reaction of NO with HO_2 SNOx is directly involved in the production of OH. SNOx also has, through O_3, an indirect influence on OH production. With OH formed by SNOx through these pathways τ_{CH_4} is decreased considerably, and the influence of SNOx on the tropospheric oxidizing efficiency is considerable, in the range of 10%.

The notable modelled influence of SNOx on directly and indirectly related trace gases shown in this work supports further efforts to improve the parameterization of SNOx in CTMs, as also proposed by Jaeglé et al. (2005).

ACPD
8, 10227–10255, 2008

Acknowledgements. We appreciate the help of the the modellers and the MESSy team, especially T. Butler, P. Jöckel, R. Sander, M. Tanarhte and H. Tost. We acknowlegde the International Max Planck Research School on Atmospheric Chemistry and Physics for financial support.

References

Bertram, T. H., Heckel, A., Richter, A., Burrows, J. P., and Cohen, R. C.: Satellite measurements of daily variations in soil NO_x emissions, Geophys. Res. Lett., 32, L24 812, doi:10.1029/2005GL024640, 2005. 10229

Brasseur, G. P., Orlando, J. J., and Tyndall, G. S. (Eds.): Atmospheric chemistry and global change, Oxford University Press, New York, 1999. 10229

Davidson, E. A. and Kingerlee, W.: A global inventory of nitric oxide emissions from soils, Nutr. Cycl. Agroecosys., 48, 37–50, 1997. 10228

Delon, C., Reeves, C. E., Stewart, D. J., Serça, D., Dupont, R., Mari, C., Chaboureau, J.-P., and Tulet, P.: Biogenic nitrogen oxide emissions from soils – impact on NO_x and ozone over West Africa during AMMA (African Monsoon Multidisciplinary Experiment): modelling study, Atmos. Chem. Phys., 8, 2351–2363, 2008, http://www.atmos-chem-phys.net/8/2351/2008/. 10229, 10230

Firestone, M. K. and Davidson, E. A.: Mikrobiological basis of NO and N_2O production and consumption in soil, In: Exchange of trace gases between terrestrial ecosystems and the atmosphere, Edited by: Andreae, M. O. and Schimel, D. S., 7–21, 1989. 10228

Ganzeveld, L. N., Lelieveld, J., Dentener, F. J., Krol, M. C., Bouwman, A. F., and Roelofs, G.-J.: Global soil-biogenic NO_x emissions and the role of canopy processes, J. Geophys. Res., 107, 4321, doi:10.1029/2001JD001289, 2002a. 10230

Ganzeveld, L. N., Lelieveld, J., Dentener, F. J., Krol, M. C., and Toelofs, G.-J.: Atmosphere-biosphere trace gas exchanges simulated with a single-column model, J. Geophys. Res., 107, 4320, doi:10.1029/2001JD000684, 2002b. 10229

Ganzeveld, L. N., van Aardenne, J. A., Butler, T. M., Lawrence, M. G., Metzger, S. M., Stier, P., Zimmermann, P., and Lelieveld, J.: Technical Note: Anthropogenic and natural offline emissions and the online EMissions and dry DEPosition submodel EMDEP of the Modular Earth Submodel system (MESSy), Atmos. Chem. Phys. Discuss., 6, 5457–5483, 2006, http://www.atmos-chem-phys-discuss.net/6/5457/2006/. 10230, 10242

Holland, E. A., Dentener, F. J., Brasswell, B. H., and Sulzman, J. M.: Contemporary and pre-industrial global reactive nitrogen budgets, Biogeochemistry, 46, 7–43, 1999. 10228
Isaksen, I. S. A. and Hov, Ø.: Calculation of trends in the tropospheric concentration of O_3, OH, CO, CH_4 and NO_x, Tellus, 39B, 271–285, 1987. 10229
Jaeglé, L., Steinberger, L., Martin, R. V., and Chance, K.: Global partitioning of NO_x sources using satellite observations: relative roles of fossil fuel combustion, biomass burning and soil emissions, Faraday Discuss., 130, 407–423, 2005. 10229, 10230, 10238
Jöckel, P., Sander, R., Kerkweg, A., Tost, H., and Lelieveld, J.: Technical Note: The Modular Earth Submodel System (MESSy) – a new approach towards Earth System Modeling, Atmos. Chem. Phys., 5, 433–444, 2005, http://www.atmos-chem-phys.net/5/433/2005/. 10230
Jöckel, P., Tost, H., Pozzer, A., Brühl, C., Buchholz, J., Ganzeveld, L., Hoor, P., Kerkweg, A., Lawrence, M. G., Sander, R., Steil, B., Stiller, G., Tanarhte, M., Taraborrelli, D., van Aardenne, J., and Lelieveld, J.: The atmospheric chemistry general circulation model ECHAM5/MESSy1: consistent simulation of ozone from the surface to the mesosphere, Atmos. Chem. Phys., 6, 5067–5104, 2006, http://www.atmos-chem-phys.net/6/5067/2006/. 10230, 10235, 10242
Kerkweg, A., Sander, R., Tost, H., and Jöckel, P.: Technical Note: Implementation of prescribed (OFFLEM), calculated (ONLEM) and pseudo-emissions (TNUDGE) of chemical species in the modular earth submodel system (MESSy), Atmos. Chem. Phys., 6, 3603–3609, 2006, http://www.atmos-chem-phys.net/6/3603/2006/. 10230, 10242
Labrador, L., von Kuhlmann, R., and Lawrence, M. G.: The effects of lightning-produced NO_x and its vertical distribution on atmospheric chemistry: sensitivity simulations with MATCH-MPIC, Atmos. Chem. Phys., 5, 1815–1834, 2005, http://www.atmos-chem-phys.net/5/1815/2005/. 10233
Labrador, L. J., von Kuhlmann, R., and Lawrence, M. G.: Strong sensitivity of the global mean OH concentration and the tropospheric oxidizing efficency to the source of NO_x from lightning, Geophys. Res. Lett., 31, L06 102, doi:10.1029/2003GL019229, 2004. 10237
Lawrence, M. G., Jöckel, P., and von Kuhlmann, R.: What does the global mean OH concentration tell us?, Atmos. Chem. Phys., 1, 37–49, 2001, http://www.atmos-chem-phys.net/1/37/2001/. 10237, 10254, 10255
Olivier, J. G. J., Bouwman, A. F., Vandermaas, C. W. M., and M, B. J. J.: Emission database for global atmospheric research (EDGAR), Environ. Monit. Assess., 31, 93–106, 1994. 10230
Sander, R., Kerkweg, A., Jöckel, P., and Lelieveld, J.: Technical note: The new comprehensive

atmospheric chemistry module MECCA, Atmos. Chem. Phys., 5, 445–450, 2005, http://www.atmos-chem-phys.net/5/445/2005/. 10242
Simpson, D.: Biogenic emissions in Europe: 2. Implications for ozone control strategies, J. Geophys. Res., 100, 22 891–22 906, 1995. 10229
Singh, H. B., Salas, L. J., and Viezee, W.: Global distribution of peroxyacetyl nitrate, Nature, 321, 588–591, 1986. 10232
Stehfest, E. and Bouwman, L.: N_2O and NO emission from agricultural fields and soils under natural vegetation: summarizing available measurement data and modeling of global annual emissions, Nutr. Cycl. Agroecosys., 24, 207–228, 2006. 10228
Steinkamp, J.: Globale Stickstoffmonoxid-Emissionen aus dem Boden: Literaturauswertung und Evaluierung des Modells ECHAM5/MESSy, Diploma thesis, Johannes-Gutenberg University, Mainz/Germany, 2007. 10231
Stockwell, D. Z., Giannakopoulos, C., Plantevin, P.-H., Carver, G. D., Chipperfield, M. P., Law, K. S., Pyle, J. A., Shallcross, D. E., and Wang, K.-Y.: Modelling NO_x from lightning and its impact on global chemical fields, Atmos. Environ., 33, 4477–4493, 1999. 10233
Taylor, K., Williamson, D., and Zwiers, F.: The sea surface temperature and sea ice concentration boundary conditions for AMIP II simulations; PCMDI Report, Tech. Rep. 60, Program for Climate Model Diagnosis and Intercomparison, 2000. 10230
Tost, H.: Global Modelling of Cloud, Convection and Precipitation Influences on Trace Gases and Aerosols, Ph.D. thesis, Rheinische Friedrich-Wilhelms-University, Bonn/Germany, 2006. 10242
Tost, H., Jöckel, P., Kerkweg, A., Sander, R., and Lelieveld, J.: Technical note: A new comprehensive SCAVenging submodel for global atmospheric chemistry modelling, Atmos. Chem. Phys., 6, 565–574, 2006a. 10242
Tost, H., Jöckel, P., and Lelieveld, J.: Influence of different convection parameterisations in a GCM, Atmos. Chem. Phys., 5475–5493, 2006b. 10242
Tost, H., Jöckel, P., and Lelieveld, J.: Lightning and convection parameterization – uncertainties in global modelling, Atmos. Chem. Phys., 4553–4568, 2007. 10242
Yienger, J. J. and Levy II, H.: Empirical model of global soil-biogenic NO_x emissions, J. Geophys. Res., 100, 11 447–11 464, 1995. 10228, 10229, 10230

Table 1. Setup of the ECHAM5/MESSy model and used submodels.

Horizontal resolution	T42 (~2.8°×2.8°)
Vertical resolution	L31 (up to 10 hPa)
Internal timestep	20 min
Timestep of output	5 h
Period of simulation	1994–1995

Used submodels	Calculation of	Literature ref.
CLOUD	Clouds and precipitation	Jöckel et al. (2006)
CONVECT	Convection	Tost et al. (2006b)
CVTRANS	Convective tracer transport	Tost (2006)
EMDEP[a]	Emission and deposition	Ganzeveld et al. (2006)
JVAL	Rates of photolysis	Jöckel et al. (2006)
LNOX	Lightning NO_x	Tost et al. (2007)
MECCA	Chemical atmospheric reactions[b]	Sander et al. (2005)
OFFLEM	Offline emissions	Kerkweg et al. (2006)
RAD4ALL	Radiation	Jöckel et al. (2006)
SCAV	Wet deposition	Tost et al. (2006a)
TNUDGE	Tracer nudging	Kerkweg et al. (2006)
TROPOP	Calculation of the tropopause	Jöckel et al. (2006)

[a] Extended version; soil NO emissions switched off in NOBIONO simulation

[b] Tropospheric reaction with NMHC and without halogens

ACPD

8, 10227–10255, 2008

Table 2. Simulated total NO_x emissions, SNOx in Tg(N) of the BASE simulation and in brackets relative contribution of SNOx to the total NO emissions for different regions and periods.

	Global		Low-latitudes (30° N–30° S)		Mid-latitudes (30° N–60° N)		(30° S–60° S)	
Season[a]	total	soil	total	soil	total	soil	total	soil
DJF	12.53	1.53 (12%)	7.09	1.34 (19%)	4.93	0.06 (1%)	0.46	0.12 (26%)
MAM	11.93	2.03 (17%)	6.07	1.60 (26%)	5.40	0.35 (6%)	0.40	0.08 (20%)
JJA	13.67	2.34 (17%)	7.04	1.43 (20%)	6.15	0.88 (14%)	0.33	0.04 (12%)
SON	13.03	1.81 (14%)	7.33	1.45 (20%)	5.27	0.29 (6%)	0.38	0.07 (18%)
All	51.17	7.72 (15%)	27.52	5.82 (21%)	21.76	1.58(7%)	1.57	0.31 (20%)

[a] DJF = December 1994, January, February 1995; MAM = March, April, May 1995; JJA = June, July, August 1995; SON = September, October, November 1995

ACPD
8, 10227–10255, 2008

Table 3. Correlation coefficient (R^2) between surface SNOx flux values and the difference (NOBIONO–BASE) of the tracer burden in the overlying lower troposphere (> 500 hPa for all gases and > 750 hPa for PAN values in brackets) by gridcell, both averaged over the corresponding period; only gridcells with a land surface fraction of at least 75% were included.

Season[a]	NO_x	PAN	HNO_3	O_3	OH	NO_x	PAN	HNO_3	O_3	OH
	Global (N=2462)					Low-latitudes 30° N–30° S (*N*=646)				
DJF	0.86	0.53 (0.60)	0.43	0.62	0.58	0.68	0.17 (0.25)	0.18	0.29	0.22
MAM	0.90	0.47 (0.53)	0.60	0.58	0.64	0.79	0.14 (0.24)	0.42	0.29	0.33
JJA	0.82	0.27 (0.35)	0.37	0.37	0.43	0.69	0.07 (0.07)	0.15	0.21	0.22
SON	0.86	0.44 (0.52)	0.43	0.55	0.58	0.66	0.14 (0.24)	0.07	0.14	0.14
Year	0.88	0.46 (0.54)	0.51	0.56	0.60	0.72	0.11 (0.23)	0.16	0.19	0.21
	Northern 30° N–60° N (*N*=637)				Mid-latitudes	Southern 30° S–60° S (*N*=46)				
DJF	0.55	0.02 (0.09)	0.40	0.07	0.31	0.80	0.45 (0.45)	0.62	0.67	0.39
MAM	0.82	0.19 (0.30)	0.43	0.20	0.27	0.76	0.71 (0.60)	0.45	0.70	0.59
JJA	0.75	0.10 (0.22)	0.26	0.13	0.18	0.83	0.46 (0.51)	0.54	0.46	0.69
AON	0.80	0.09 (0.19)	0.40	0.19	0.32	0.87	0.74 (0.77)	0.65	0.77	0.47
Year	0.77	0.12 (0.23)	0.33	0.16	0.16	0.79	0.66 (0.65)	0.64	0.78	0.56

[a] See Table 2 for abbreviations

ACPD
8, 10227–10255, 2008

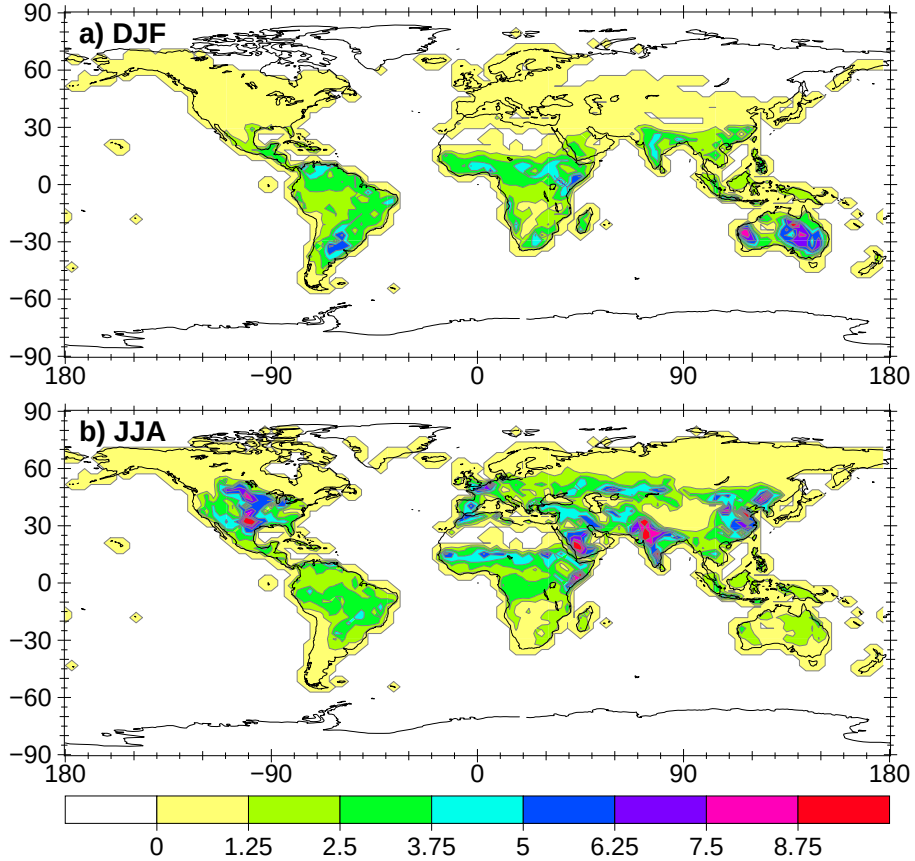

Fig. 1. Simulated SNOx flux for **(a)** December 1994 to February 1995 and **(b)** June to August 1995 in $\frac{ng}{m^2 s}$.

ACPD
8, 10227–10255, 2008

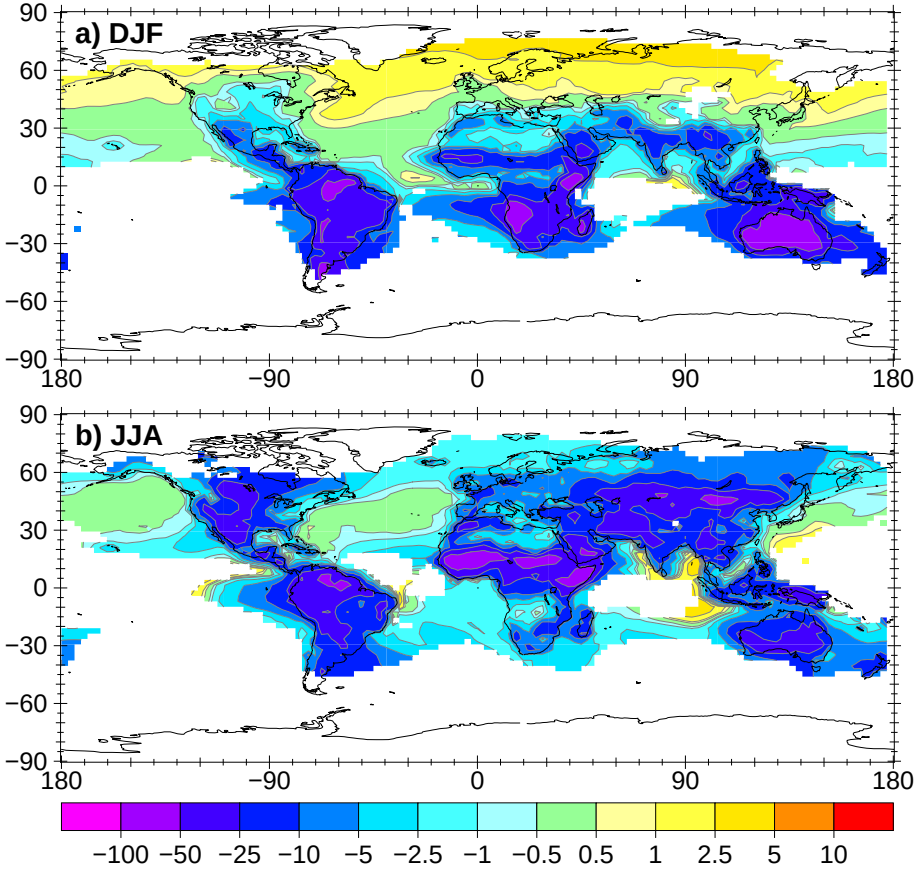

Fig. 2. Relative difference ($\frac{\text{NOBIONO}-\text{BASE}}{\text{BASE}} \times 100\%$) of the lower tropospheric mixing ratio of NO_x in % – values below 30 $\frac{\text{pmol}}{\text{mol}}$ in the BASE simulation excluded from calculation – averaged for **(a)** December, January, February and **(b)** June, July and August.

ACPD
8, 10227–10255, 2008

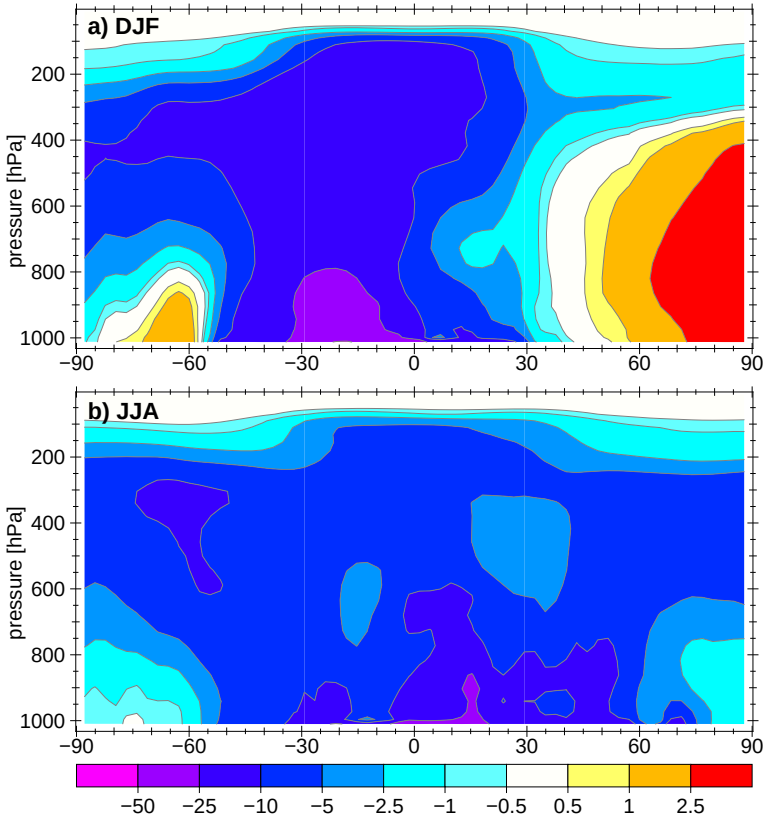

Fig. 3. Zonal mean relative difference ($\frac{\text{NOBIONO}-\text{BASE}}{\text{BASE}} \times 100\%$) of NO_x mixing ratio in % averaged for **(a)** December, January, February and **(b)** June, July and August. Note that the y-axis is linearly scaled, since the focus of this work lies in the lower troposphere.

ACPD
8, 10227–10255, 2008

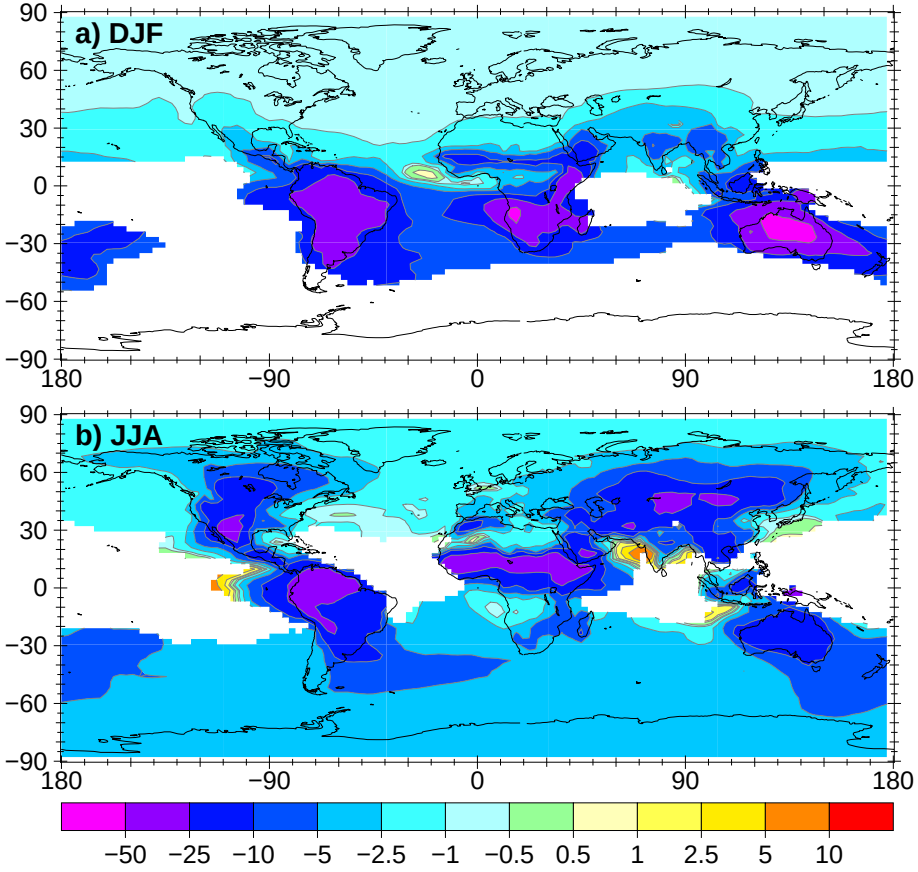

Fig. 4. Relative difference ($\frac{\text{NOBIONO}-\text{BASE}}{\text{BASE}} \times 100\%$) of the lower tropospheric mixing ratio of PAN in % – values below 50 $\frac{\text{pmol}}{\text{mol}}$ in the BASE run excluded from calculation – averaged for **(a)** December, January, February and **(b)** June, July and August.

ACPD
8, 10227–10255, 2008

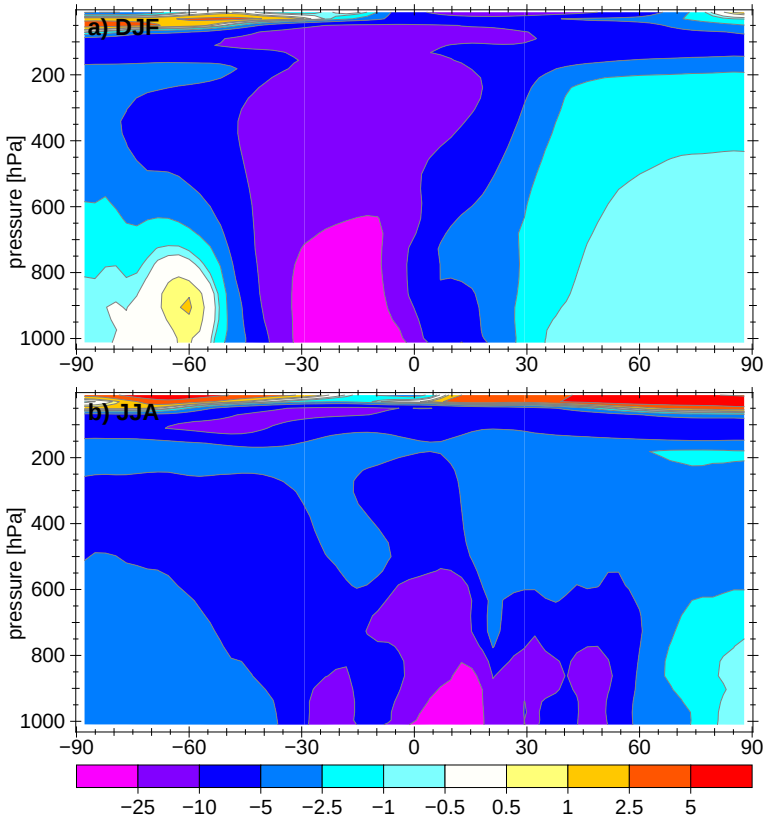

Fig. 5. Zonal mean relative difference ($\frac{\text{NOBIONO}-\text{BASE}}{\text{BASE}} \times 100\%$) of PAN mixing ratio in % averaged for **(a)** December, January, February and **(b)** June, July and August.

ACPD
8, 10227–10255, 2008

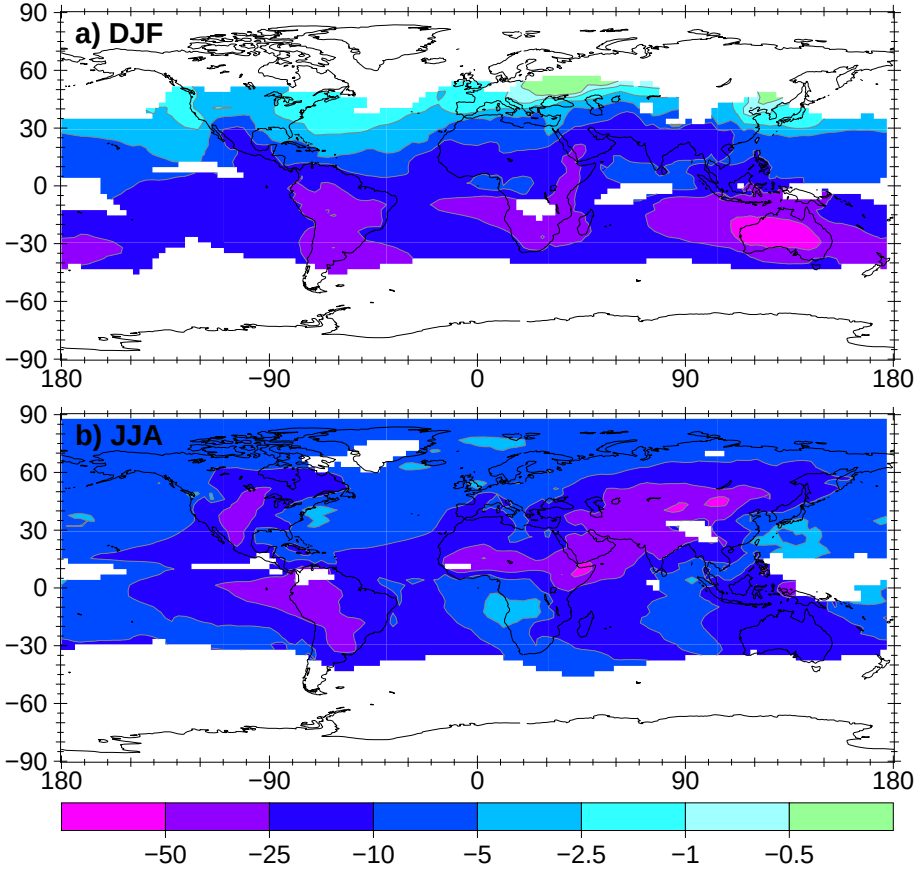

Fig. 6. Relative difference ($\frac{\text{NOBIONO}-\text{BASE}}{\text{BASE}} \times 100\%$) of the lower tropospheric mixing ratio of HNO_3 in % – values below 30 $\frac{\text{pmol}}{\text{mol}}$ in the BASE simulation excluded from calculation – averaged for **(a)** December, January, February and **(b)** June, July and August.

ACPD
8, 10227–10255, 2008

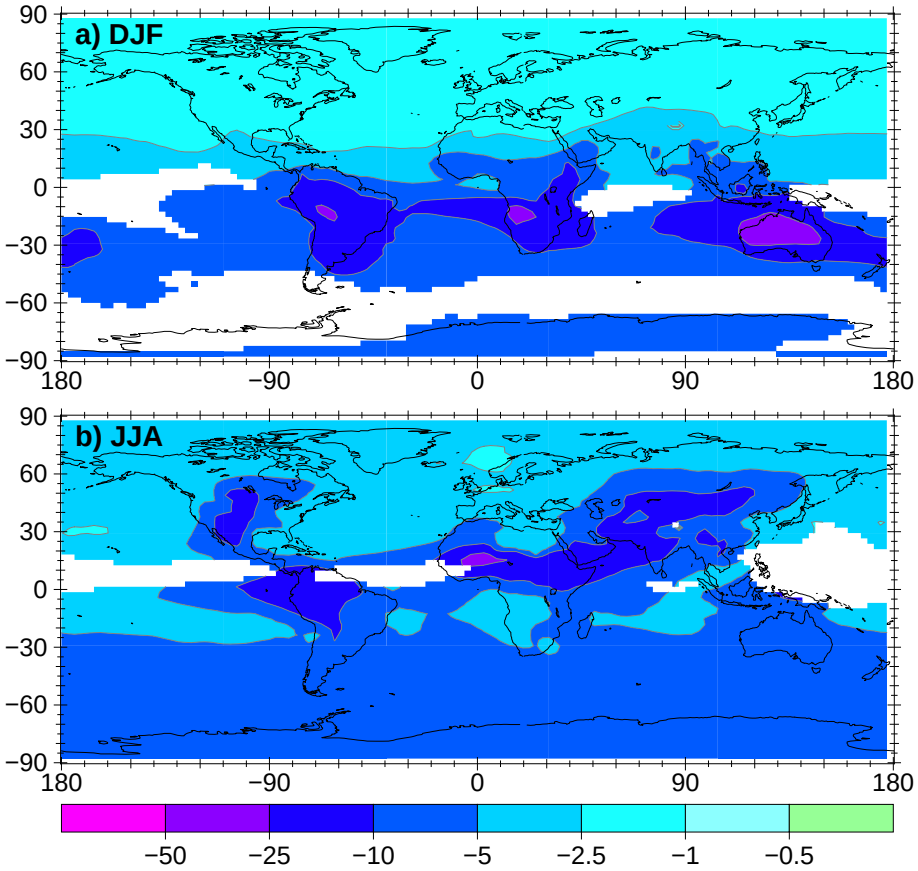

Fig. 7. Relative difference ($\frac{\text{NOBIONO}-\text{BASE}}{\text{BASE}} \times 100\%$) of the lower tropospheric mixing ratio of O_3 in % – values below 25 $\frac{\text{nmol}}{\text{mol}}$ in the BASE simulation excluded from calculation – averaged for **(a)** December, January, February and **(b)** June, July and August.

ACPD
8, 10227–10255, 2008

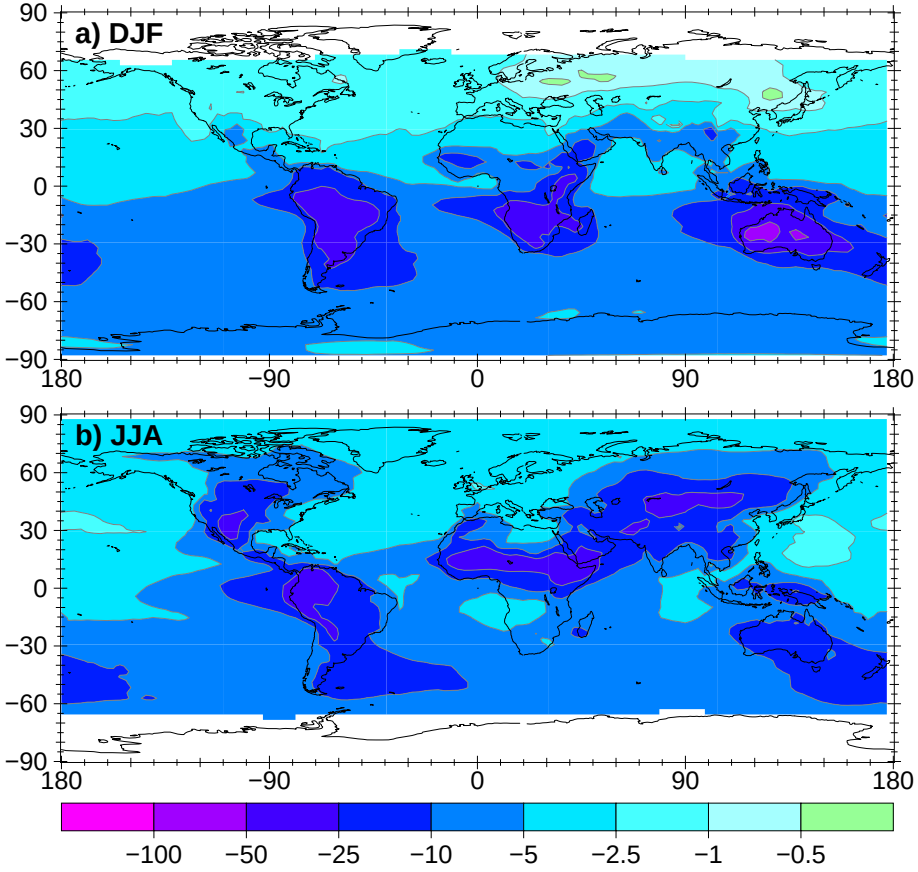

Fig. 8. Relative difference ($\frac{\text{NOBIONO}-\text{BASE}}{\text{BASE}} \times 100\%$) of the lower tropospheric concentration of OH in % – values below $10^4 \frac{\text{molec}}{\text{cm}^3}$ in the BASE simulation excluded from calculation – averaged for **(a)** December, January, February and **(b)** June, July and August.

ACPD
8, 10227–10255, 2008

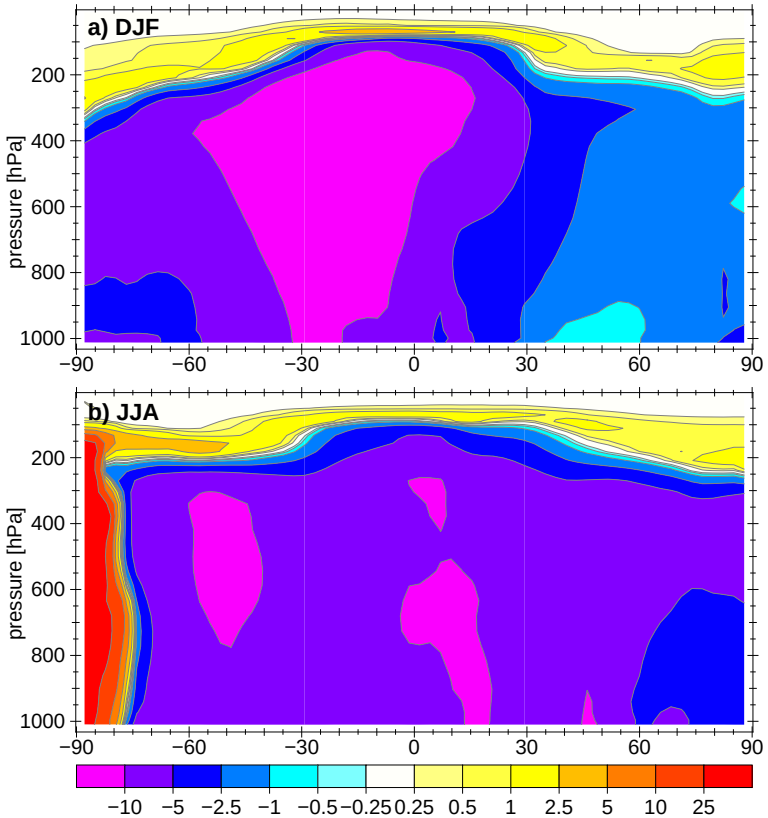

Fig. 9. Zonal mean relative difference ($\frac{\text{NOBIONO}-\text{BASE}}{\text{BASE}} \times 100\%$) of OH mixing ratio in % averaged for **(a)** December, January, February and **(b)** June, July and August.

ACPD
8, 10227–10255, 2008

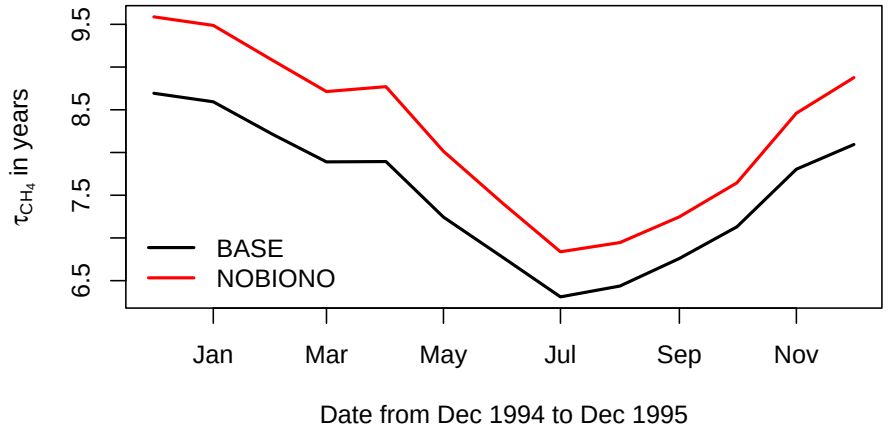

Fig. 10. Seasonal cycle of monthly mean lifetime of CH_4 from December 1994 to December 1995 in years (calculated according to Lawrence et al., 2001).

ACPD
8, 10227–10255, 2008

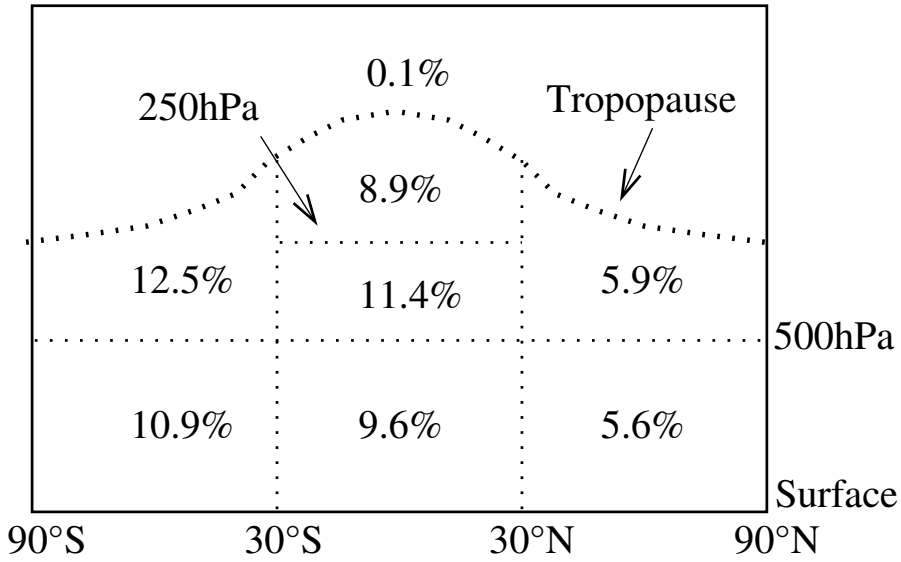

Fig. 11. Relative increase of τ_{CH_4} ($\frac{\tau_{CH_4,NOBIONO}-\tau_{CH_4,BASE}}{\tau_{CH_4,BASE}} \times 100\%$) in various zonal subdomains of the atmosphere (calculated after Lawrence et al., 2001).

ACPD
8, 10227–10255, 2008